Crack tip shape effect on stress-strain fields in plastically compressible materials

IOP Conf. Series: Materials Science and Engineering **629** (2019) 012035 doi:10.1088/1757-899X/629/1/012035

Crack tip shape effect on stress-strain fields in plastically compressible materials

M I Alam[1], D Khan[1,2], Y Mittal[1] and S Kumar[1]

[1]Department of Mechanical Engineering, Indian Institute of Technology (BHU) Varanasi, Varanasi - 221005, India

E-mail: dkhan.mec@itbhu.ac.in

Abstract. In the present study, the effects of crack tip shape on near tip deformation and fields are numerically investigated for a mode I crack under plane strain and small scale yielding conditions. The material is characterized by finite strain elastic-viscoplastic constitutive relation with bi-linear hardening and hardening-softening-hardening hardness functions. Both plastically incompressible and compressible solids have been considered for analyses. It has been observed that the combination of crack tip profile and plastic compressibility has significant effect on the near tip deformation and plastic fields.

1. Introduction

In several numerical simulations based on initially sharp crack tip it has been observed that severe blunting takes place in the very early stages of crack tip plasticity and consequently it leads to a highly distorted mesh. Therefore, in numerical simulation, people mostly use originally blunted crack having a circular arc tip [1]. However, in practical situation it is observed that the crack tip is neither exactly circular nor completely sharp, but of arbitrary shape with a finite amount of curvature. In recent times, in the study of fracture in solids, the effect of crack-tip shape has attracted notable research attention.The notch root radius effect on fracture toughness was examined for a variety of brittle and ceramic materials in [2-4] and it was noticed that the root radius can have impact on the fracture toughness significantly. Further, experimentation of notch tip radius on fatigue crack growth for two different alloys was performed in [5] and it was concluded that for blunter notch the fatigue crack growth rate is more. Also, it is reported in literature that with increase in the crack-tip curvature radius, near crack-tip plastic strain as well as stresses increase considerably in glassy polymer [6].For elastomers, some studies on crack growth and the associated changes in crack-tip shapes have been reported in [7].

Some of the results obtained from the experimentation analysis on the behavior of materials like metallic foams, transformation toughened ceramics and plastics suggest that the constitutive equations of these materials comprise pressure-sensitive yielding. Due to some impressive mechanical properties, these materials have attracted numerous researchers over the past several years. For understanding the deformation and stress-strain fields near a crack tip in pressure sensitive and/or plastically compressible solids, a large amount of research works has been done, in recent times, for both monotonic and fatigue loadings. It should be mentioned here that most of these studies are based on small deformation and only a few studies are founded on large deformation formulation [8-13]. Considering potential applications of the above mentioned materials, it appears that it is required to look into the influence of notch or crack-tip shape on near tip deformation and fields for the above mentioned materials. Plastic normality; plane strain and small scale yielding conditions have been assumed in the present computations.

2. Constitutive equation

The material model used here is same as that given in [8-13].The elastic part of the deformation is expressed as

$$\mathbf{d}^{e} = \mathbf{L}^{-1}\colon\hat{\boldsymbol{\tau}} = \frac{1+\nu}{E}\hat{\boldsymbol{\tau}} - \frac{\nu}{E}\mathrm{tr}(\hat{\boldsymbol{\tau}})\mathbf{I} \tag{1}$$

Where, **L** is the elastic moduli tensor,$\hat{\boldsymbol{\tau}}$ is the Jaumann rate of Kirchhoff stress, *E* and *v* are the Young's modulus and Poisson's ratio, respectively, tr(.)indicates the trace and **I** the identity tensor, **A**: **B**=$A_{ij}B_{ij}$.

The plastic part of the deformation is expressed as

$$\mathbf{d}^{p} = \frac{3}{2}\frac{\dot{\varepsilon_p}}{\sigma_e}\mathbf{p} \tag{2}$$

Where, $\dot{\epsilon}_{\mathrm{p}}$ is plastic strain rate and σ_{e} is effective stress corresponding to the instantaneous $\dot{\epsilon}_{\mathrm{p}}$ and **p** is deviatoric part of Kirchhoff stress tensor. The **p** is given by

$$\mathbf{p} = \boldsymbol{\tau} - \alpha\mathrm{tr}(\boldsymbol{\tau})\mathbf{I} \tag{3}$$

When $\alpha = 1/3,$ the equation (3) is reduced to constitutive relation for isotropic hardening viscoplastic Mises solid. In this work,we use the following viscoplastic strain rate relation

$$\dot{\epsilon}_{\mathrm{p}} = \dot{\epsilon}_0\left(\frac{\sigma_{\mathrm{e}}}{\mathrm{g}}\right)^{1/m} \tag{4}$$

Where, $\dot{\varepsilon}_0$ and *m* represent the reference strain rate and the hardening exponent, respectively; the hardening function g is written as

$$\mathrm{g}(\epsilon_{\mathrm{p}}) = \sigma_0\begin{cases} 1+h_1\epsilon_{\mathrm{p}}, & \epsilon_{\mathrm{p}} < \epsilon_1 \\ 1+h_1\epsilon_1 + h_2(\epsilon_{\mathrm{p}}-\epsilon_1), & \epsilon_1 < \epsilon_{\mathrm{p}} < \epsilon_2 \\ 1+h_1\epsilon_1 + h_2(\epsilon_2-\epsilon_1) + h_3(\epsilon_{\mathrm{p}}-\epsilon_2), & \epsilon_{\mathrm{p}} > \epsilon_2 \end{cases} \tag{5}$$

Where, σ_0 is a reference stress. The effective stress, σ_{e} is defined by

$$\sigma_{\mathrm{e}}^2 = \frac{3}{2}\boldsymbol{\tau}\colon\mathbf{p} = \frac{3}{2}\left[\boldsymbol{\tau}\colon\boldsymbol{\tau} - \alpha\left(\mathrm{tr}(\boldsymbol{\tau})\right)^2\right] \tag{6}$$

3. Problem formulation

The field equations, used in this work, are functions of convected coordinates, $y^{\mathrm{i}}$and time (t) [8-13]. The principle of virtual work in absence of body force and for quasi-static deformation can be written as

$$\int_{\mathrm{V}}\tau^{\mathrm{ij}}\,\delta E_{\mathrm{ij}}dV = \int_{\mathrm{S}}T^{\mathrm{i}}\,\delta u_{\mathrm{i}}dS \tag{7}$$

Where, V and S represent the volume and surface of the body in the reference configuration, τ^{ij} are the Kirchhoff stress in the deformed convected coordinate, E_{ij} the Lagrangian strain, T^{i} the nominal traction and u_{i} are the displacement components.

From the above equation (7), the incremental equilibrium is obtained as

$$\Delta t\int_{\mathrm{V}}\left(\dot{\tau}^{\mathrm{ij}}\delta E_{\mathrm{ij}} + \tau^{\mathrm{ij}}\dot{u}^{\mathrm{k}}_{,\mathrm{i}}\delta u_{\mathrm{k,j}}\right)dV = \Delta t\int_{\mathrm{S}}\dot{T}^{\mathrm{i}}\,\delta u_{\mathrm{i}}dS - \left[\int_{\mathrm{V}}\tau^{\mathrm{ij}}\,\delta E_{\mathrm{ij}}dV - \int_{\mathrm{S}}T^{\mathrm{i}}\,\delta u_{\mathrm{i}}dS\right] \tag{8}$$

In equation (8), the term $\left[\int_{\mathrm{V}}\tau^{\mathrm{ij}}\,\delta E_{\mathrm{ij}}dV - \int_{\mathrm{S}}T^{\mathrm{i}}\,\delta u_{\mathrm{i}}dS\right]$ stands for an equilibrium correction term.

4. Finite element model and some numerical results

In the present finite element simulation, the numerical results are generated for the geometry as shown in figure 1, where the outer radius (R_∞) is 2.0 in any arbitrary units. Motivated by the works of Li *et al*. [6], here, we use a similar type of elliptical arc to describe the crack tip profile. The semi-major and semi-minor axes of the ellipse are represented by a and b in the same arbitrary units, respectively and the ratio a/b specifies the crack shape as shown in figure 1. The constant loading rate is $\dot{K_I}/\sigma_0\dot{\varepsilon_0}\sqrt{b} = 31.62$, where $\dot{K}_I = 1\ MPa\sqrt{m}s^{-1}$. In order to calculate the deformation history, linear increments are used with time step size of 0.0002.

Quadrilateral elements are used for grid generation and each quadrilateral is made of four crossed triangular elements with constant strain. To reproduce the localized deformation pattern at finite strains, such elements are widely used [10-13]. In the present analysis, after carrying out the mesh convergence study with meshes consisting of 28 x 64, 28 x 74 and 28 x 84 quadrilateral elements, the mesh density finally has been fixed at28 x 74 quadrilateral elements. The near tip plastic strain contours were compared and it was noticed that the results from 28 x 74 and 28 x 84 were in good agreement.

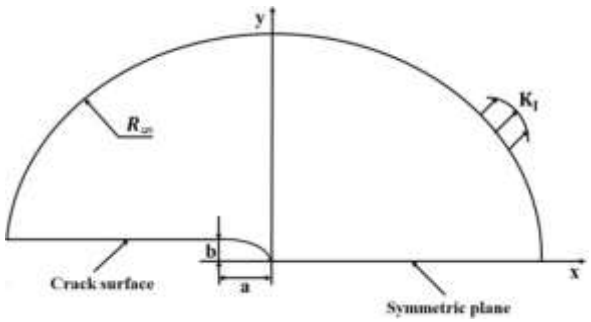

Figure 1. Schematic view of the elliptical crack tip used for simulation in finite element analyses.

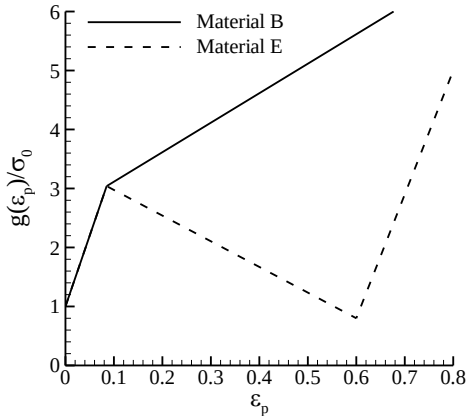

Figure 2. Graph of hardness function $g(\varepsilon_p)$ for materials B and E, [10].

In this study, materials B and E from [10] are considered and the hardness functions of those materials are shown in figure 2. Material B is a bilinear hardening material whereas material E is a trilinear hardening-softening-hardening solid. At $\varepsilon_1$the material B starts re-hardening whereas at the same plastic strain softening takes place in material E. The value of ε_2 defines the plastic strain at which material E starts again hardening after the softening. The values of h_1 and ε_1 are same for the two materials and those are 24 and 0.085, respectively; also h_2 and h_3 are same for material B and it is 5.0 whereas for material E, h_2 is -3.90 and h_3 is 15.0. The other constant material parameters are E/σ_0=100, $\dot{\varepsilon}_0$=1 and m = 0.02.

At the remote outer boundary of the semi-circle, K_I field displacements are imposed. Here, traction free crack surfaces are assumed and on line $y^2 = 0$, symmetry boundary conditions are applied; in the present case $y^2 = y$. For the constitutive update, rate tangent modulus method by Peirce *et al* [14] is considered here.

4.1. Near-tip normal stress (σ_{yy}) distributions

Figures 3 – 4 illustrate the normal stress (σ_{yy}) variations in front of the crack tip along the x-axis for materials B and E where the three crack shapes specified by a/b = 1 ,4 and 8 are considered. Both plastically incompressible and compressible solids have been considered for analyses. It is reflected from all the figures that near tip stresses vary with the crack tip distance and also the three crack tip shapes influence these stress fields differently. The stress quantities become almost constant as we move far from the crack tip. There is considerable amount of increase in the values of σ_{yy} as we increase the

curvature radius at crack tip and also the far field stress from the tip becomes independent of the crack tip shape. For both the materials, when these are plastically compressible, the maximum stress is reduced than that of plastically incompressible solid. Also for plastically compressible solids, there are kinks, which are slightly away from the tip, and it may be due to the formation of shear band as would be shown in the subsequent figures. The location of these kinks depends on the crack tip shapes. For material E, because of the softening, the maximum stress is further reduced as compared to that of material B.

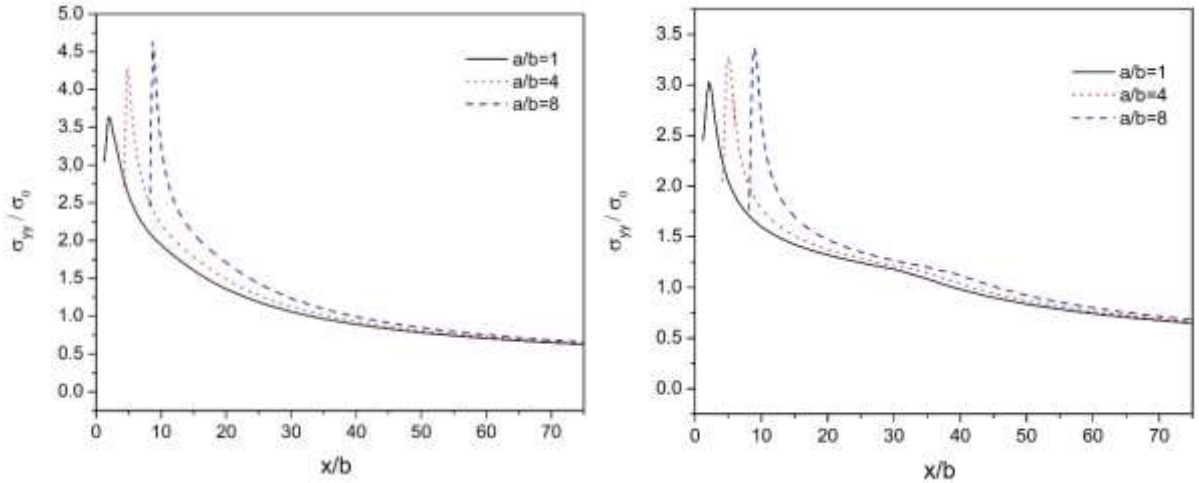

(a) (b)

Figure 3. Variation of normal stress (σ_{yy}) just ahead of the tip**,** material B, under $J_{app}/(\sigma_0 b)$ =1.6; (a) plastically incompressible solid and (b) plastically compressible solid ($\alpha = 0.28$).

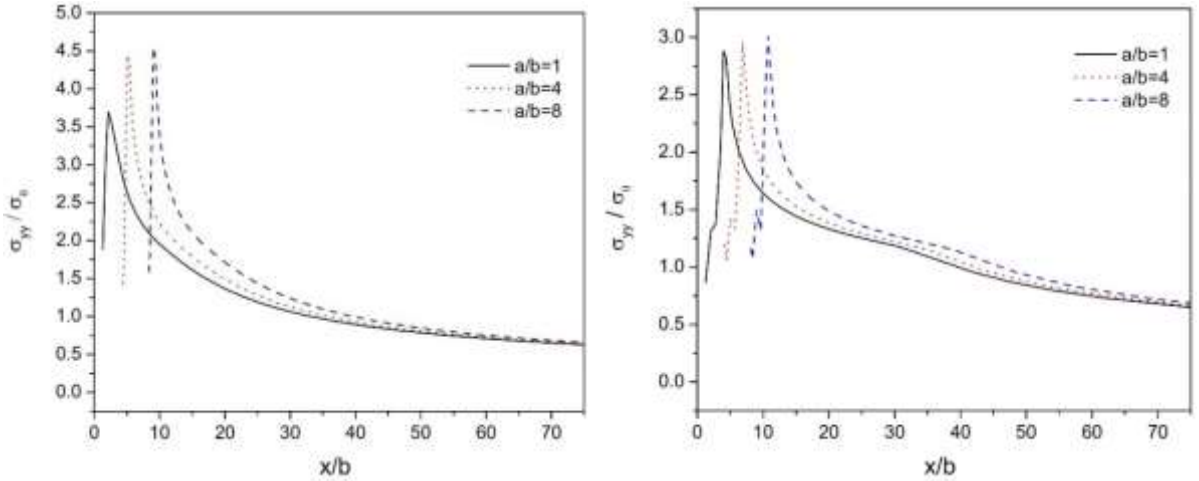

(a) (b)

Figure 4. Variation of normal stress (σ_{yy}) just ahead of the tip, material E, under $J_{app}/(\sigma_0 b)$ =1.6; (a) plastically incompressible solid and (b) plastically compressible solid ($\alpha = 0.28$).

4.2. Accumulated plastic strain distributions

Figures 5 – 8 illustrate the distributions of plastic strain in materials B and E for the two crack shapes, i.e. with a/b= 1 and 8 and at same load level, i. e. $J_{app}/(\sigma_0 b) = 1.6$. It is apparent that crack tip shape, plastic compressibility and material softening have significant effect on the near tip plastic deformation. In figure 5, the intense plastic deformation is limited to a very small region around the tip due to the

material strain hardening. As, the ratio of a/b increases, the zone of intense plastic deformation decreases along the vertical axis, and the stress concentration is increased on the crack tip. It is also to be noted here that with increase of the curvature radius at tip, the outer kidney shaped contour is tilted in a clockwise sense for the incompressible solid. For plastically compressible solid with $\alpha = 0.28$, it is observed from figure 6 that the extent of severe stain region increases at the crack tip when the curvature radius is more.

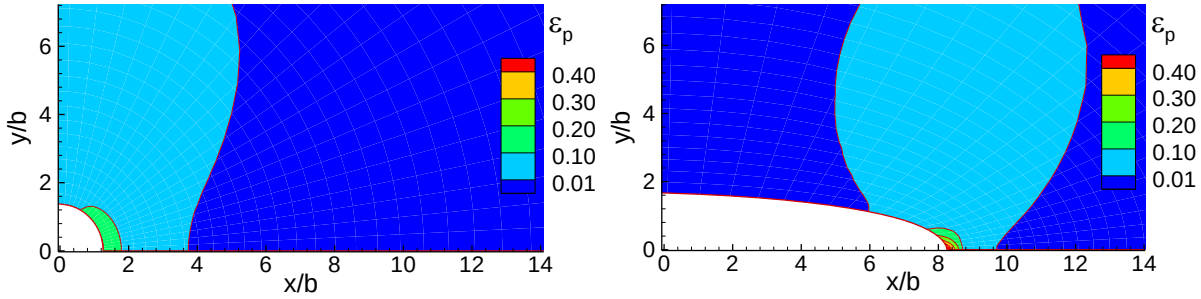

Figure 5. Near tip plastic strain field, material B at $J_{app}/(\sigma_0 b)) = 1.6$ for plastically incompressible solid; (a) a/b= 1and (b) a/b= 8.

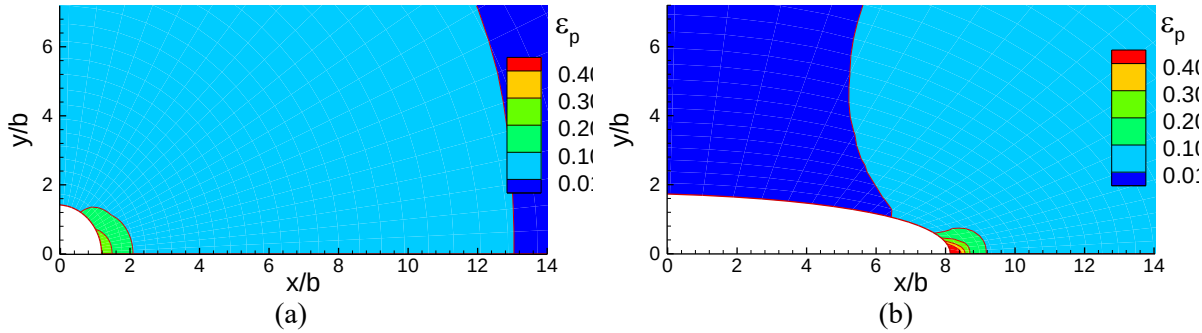

Figure 6. Near tip plastic strain field, material B at $J_{app}/(\sigma_0 b)) = 1.6$ for plastically compressible solid ($\alpha = 0.28$); (a) a/b= 1 and (b) a/b= 8.

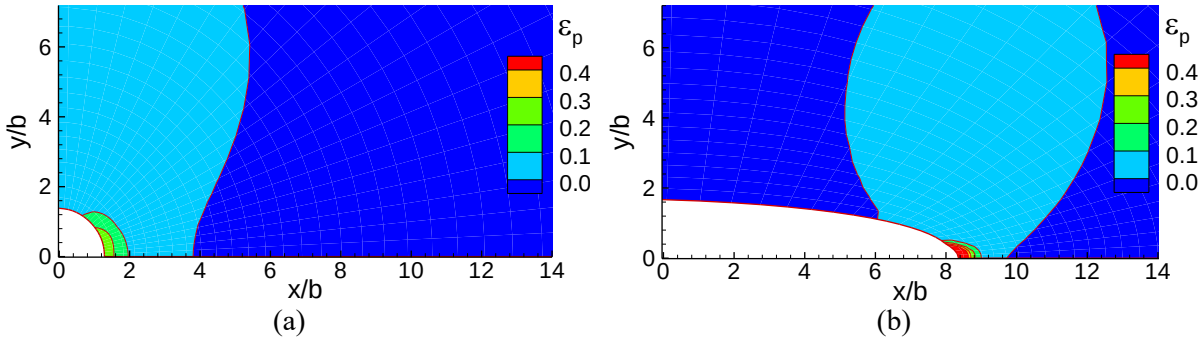

Figure 7. Near tip plastic strain field, material E at $J_{app}/(\sigma_0 b)) = 1.6$ for plastically incompressible solid; (a) a/b= 1 and (b) a/b= 8.

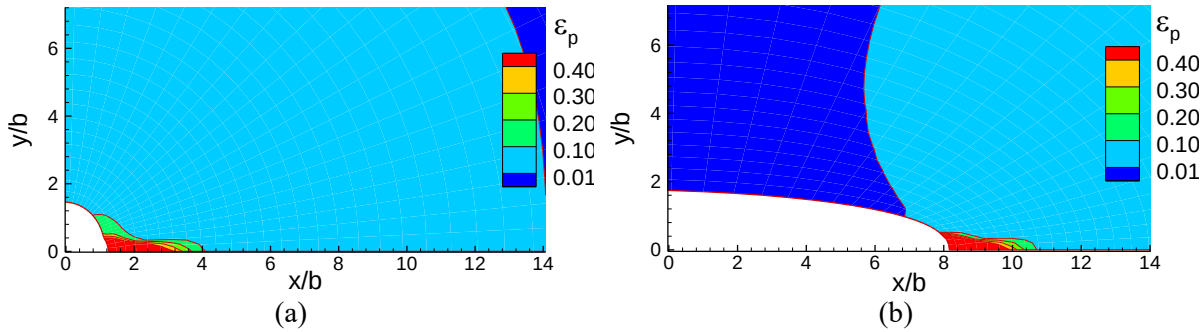

Figure 8. Near tip plastic strain field, material E at $J_{app}/(\sigma_0 b)) = 1.6$ for plastically compressible solid ($\alpha = 0.28$); (a) a/b= 1 and (b) a/b= 8.

While in figures 5, 6 and 7, the plastic strain is maximum on the blunting surface of the crack, however, the plastic compressibility, material softening and the shape of crack tip have a major consequence on the plastic strain distribution in material E. The zone of intense strain region in material E originates from the crack surface near the symmetry plane. Even though, in material E due to the material softening, localization of the shear band is common to both the two crack shapes, figures 7 and 8, however, it is reflected that for the sharper crack tip, the plastic strain concentration near the tip is slightly more at the present load level.

5. Conclusions

In the present study, the influence of the shape of a crack tip on the near tip deformation and stress-strain fields has been examined. For the investigation purpose, finite element finite deformation study has been conducted where the material is characterized by an elastic viscoplastic constitutive relation with a hardening and hardening-softening-hardening hardness functions. In the analysis, plane strain deformation, mode I loading and small scale yielding conditions have been assumed. The combination of crack tip shape, plastic compressibility and material softening shows the way to main variations in the stress and deformation fields near the tip. The finite element results show that there is considerable amount of increase in the values of σ_{yy} as we increase the curvature radius at crack tip. Also because of plastic compressibility as well as material softening, the maximum normal stress is reduced significantly. It is also revealed that as the curvature radius increases, the intense plastic deformation approaches to crack tip. Furthermore, the presence of plastic compressibility and material softening influences the localization near the crack tip differently depending on the crack tip shape.

References

[1] McMeeking RM 1977 Finite deformation analysis of crack tip opening in elastic-plastic materials and implications for fracture nanotubes *J. Mech. Phys. Solids* **25** 357-81
[2] Nishida T and Hanaki Y 1994 Effect of notch-root radius on the fracture toughness of a fine-grained alumina *J. American Cer. Soc.* **77** 606-8
[3] Damani R, Gstrein R and Danzer R 1996 Critical notch-root radius effect in SENB-S fracture toughness testing *J. Euro. Cer. Soc.* **16** 695-702
[4] Picard D, Leguillon C and Putot C 2006 A method to estimate the influence of tge notch-root radius on the fracture toughness measurement of ceramics *J. Euro. Cer. Soc.* **26** 1421-7
[5] Rozumek D, Macha E, Lazzarin P and Meneghetti G 2006 Influence of notch (tip) radius on fatigue crack growth rate *J. Theo. Appl. Mech.* **44** 127-37
[6] Li H, Wang G and Wang T J 2008 Effect of crack-tip-shape on the near-tip field in glassy polymer *Int. J. Solids Struct.* **45** 1087-100
[7] Morishita Y, Tsunoda K and Urayama K 2017 Crack-tip shape in the crack growth rate transition of filled elastomers *Polymer***108** 230-41
[8] Hutchens S B, Needleman A and Greer J R 2011 Analysis of uniaxial compression of vertically

aligned carbon nanotubes *J. Mech. Phys. Solids* **59** 2227-37
[9] Needleman A, Hutchens S B, Mohan N and Greer J R 2012 Deformation of plastically compressible hardening–softening–hardening solids *Acta Mech. Sin.* **28** 1115-24
[10] Mohan N, Cheng J, Greer J R and Needleman A 2013Uniaxial tension of a class of compressible solids with plastic non-normality *J. Appl. Mech.* **80** 040912-1-8
[11] Singh S and Khan D 2018 On fatigue crack growth in plastically compressible hardening and hardening-softening-hardening solids using crack tip blunting *Int. J. Fract.* **213** 139-55
[12] Khan D, Singh S and Needleman A 2017 Finite deformation analysis of crack tip fields in plastically compressible hardening – softening – hardening solids *Acta Mech. Sin.* **33** 148-58
[13] Singh S and Khan D 2018 Quasi-statically growing crack tip fields in plastically compressible hardening-softening-hardening solid *Int. J. Struct. Integ.* **9** 532-47
[14] Peirce D, Shih C F and Needleman A 1984 A tangent modulus method for rate dependent solids *Comp. Struct.* **18** 875-87